ISSN 2070-0482, Mathematical Models and Computer Simulations, 2018, Vol. 10, No. 5, pp. 551–563. © Pleiades Publishing, Ltd., 2018.
Original Russian Text © M.V. Skachkov, 2018, published in Matematicheskoe Modelirovanie, 2018, Vol. 30, No. 2, pp. 18–32.

Application of the Monte Carlo Method for Simulation of Pattern Formation by Ion-Beam Sputtering of Amorphous Bodies

M. V. Skachkov*

National Research Nuclear University MEPhI (Moscow Engineering Physics Institute), Moscow, 115409 Russia
**e-mail: mvskachkov@mephi.ru*

Received January 30, 2017

Abstract—The formation of ordered structures by ion-beam sputtering of a surface of an amorphous body in the case when a strong nonlinearity has a significant effect on the morphology of the irradiated surface is studied. Three modifications of the Monte Carlo method are used for the numerical simulation of the process, and the first of them is a kind of imitational simulation. It is shown that the direct (imitating) statistical simulation of the ion bombardment of the surface of the target, which best matches the considered physical process and is widely used in other papers, has a serious disadvantage. In the case of imitational simulation, random fluctuations of the depth of the sputtering roughen the target surface to such an extent that none of the modes provided by the continuous model can be observed. It especially concerns the modes set after the long ion bombardment of the surface of the target. However, solutions of the continuous model can be investigated numerically by means of other modifications of the Monte Carlo method with decreased dispersion. Two of these modifications are developed in this paper. Applying these methods, under certain conditions, an ordered structure composed of hexagonally symmetrical hollows is obtained on the surface of the target after the target's long-term exposure to irradiation by a normal ion beam.

Keywords: erosion velocity, ion-beam sputtering, Monte Carlo method, surface diffusion, hexagonal symmetry, structural factor, surface width

DOI: 10.1134/S2070048218050113

1. INTRODUCTION

Numerous experiments [1, 2] show the formation of ripples on the surfaces of metals and semiconductors at an oblique incidence of the ion beam, and they show ordered structures composed of hexagonally symmetrical hollows or dots when the ion beam falls normally. Many papers [2–7] are devoted to theoretical studies of this phenomenon. Some of them are based on the following continuous model: time variations of the height of the irradiated surface $h(x, y, t)$ above the point of the plane (x, y) are described by the following equation [2]:

$$\frac{\partial h}{\partial t} = -V_0\sqrt{g} - K\nabla^4 h + \eta(x, y, t), \tag{1}$$

where V_0 is the erosion velocity directed towards the interior normal to the surface; $g = 1 + (\partial_x h)^2 + (\partial_y h)^2 = \cos^{-2}\psi$; ψ is the angle between the normal line to the surface at the point $(x, y, h(x, y, t))$ and axis z; K is the coefficient of surface diffusion; and $\eta(x, y, t)$ is the random noise with zero mathematical expectation. The erosion velocity is proportional to the ion energy absorbed at unit time in the unit volume near point $(x, y, h(x, y, t))$:

$$V_0 = -\Lambda\iint \mathbf{J}\cdot\mathbf{n}'\cdot E(x, y, h(x, y, t), x', y', h(x', y', t))dS', \tag{2}$$

where $\mathbf{J}$ is the averaged density of the ion flow; $\mathbf{n}'$ is the outer normal to the irradiated surface at the point $(x', y', h(x', y', t))$; $E(x, y, h(x, y, t), x', y', h(x', y', t))$ is the energy absorbed in unit volume near the point $(x, y, h(x, y, t))$ as a result of the ion's interaction with the target surface at the point $(x', y', h(x', y', t))$; dS' is an element of the target surface at the point $(x', y', h(x', y', t))$; and Λ is the proportionality coefficient.

Generally, the integro-differential Eqs. (1) and (2) is complicated for the theoretical analysis. Almost in all papers, the authors use the Gaussian approximation of the absorbed ion energy proposed by Sig-

mund for the ionic sputtering of amorphous body surfaces [8], and simplify Eqs. (1) and (2) to reduce it to a stochastic nonlinear differential equation of the fourth or the sixth order [2–7]. The theoretical and numerical studies of the properties of these simplified models has allowed us to specify the basic modes of ripple formation on the surface of amorphous bodies depending on the angle of incidence of the ion beam, and the formation of hollows or dots at the normal incidence of the ion beam. However, solutions of the continuous model of Eqs. (1) and (2) remain insufficiently studied at the times when strong nonlinearity renders significant influence on the morphology of the irradiated surface. In particular, the possibility of the formation of ordered structures composed of hexagonally symmetrical hollows has not been studied applying models (1) and (2).

In this respect, numerical studies of models (1) and (2) or its discrete analogs using the statistical simulation methods (Monte Carlo) [9–11] are pertinent. The known discrete models applied to solve this problem (see, for example, [12, 13]), engage direct (imitational) statistical simulation, which considers true ion trajectories, whose coordinates are drawn in the incident flow as random points uniformly distributed in a certain region. Note that the ripple wavelength observed on the surface of the target is about a few hundredths of a μm; i.e. the calculation area of the considered surface of the target should be about few tenths of a μm. The ion flow falling onto this area can be about 10^7–10^{13} ion/min. Simulation of all particle interactions with the surface of the target involves huge computational costs. In the calculation experiments, we can reduce the density of the ion flow artificially by increasing the proportionality factor Λ in (2) and maintaining the erosion velocity, i.e., ensuring the fulfillment of equality $\Lambda \cdot |\mathbf{J}| = \text{const}$. This approach results in an overestimation of the statistical error of the calculation results. It is shown in [14] that if the random depth fluctuations of the target sputtering are rather large, they destroy the wave structure on the target surface. Therefore, it is expedient to use other modifications of the Monte Carlo method for the numerical study of models (1) and (2).

In this paper, three modifications of the Monte Carlo method are considered for the numerical study of models (1) and (2), and the first one is of the imitational simulation type. The results of the calculations obtained by using these modifications are compared. An ordered structure of hexagonally symmetrical hollows is formed after lengthy bombardment with a normal ion beam under certain conditions. It is shown that the first modification of the Monte Carlo method (imitational simulation) does not provide the specified mode under limited computing resources, due to the high random fluctuations of the depth of the target sputtering.

2. FORMULATION OF THE PROBLEM

The collimated monoenergetic ion beam's incidence onto the plane surface of the target is considered. The time evolution of the morphology of the target surface is described by the following equation:

$$\frac{\partial h}{\partial t} = -V_0\sqrt{g} - D\left(\frac{\partial^4 h}{\partial x^4} + \cos^4\theta\frac{\partial^4 h}{\partial y^4} + 2\cos^2\theta\frac{\partial^4 h}{\partial x^2\partial y^2}\right), \tag{3}$$

where $g = 1 + (\partial_x h)^2 + (\partial_y h)^2$,

$$V_0(x,y,t) = \Lambda\int_{-\infty}^{+\infty}\int_{-\infty}^{+\infty} dx'dy'\Phi(x',y',t)E(x-x',y-y',h(x,y,t)-h(x',y',t)+a),$$
$$E(x,y,z) = \frac{1}{(2\pi)^{3/2}\mu^2\sigma}\exp\left\{-\frac{z^2}{2\sigma^2} - \frac{x^2+y^2}{2\mu^2}\right\}, \tag{4}$$

a is the ion mean penetration into the target material, $\Phi(x,y,t)$ is the ion flow density perpendicularly to the xy plane, D is the coefficient of the surface diffusion, and θ is the angle between the plane of the target and the xy plane (x axis is parallel to the target plane). When $\theta = 0$, the ion incidence onto the target surface is normal. Note that other papers consider this angle as zero, while considering the angle between the flow density vector and the z axis as nonzero. In this case, the inequality $\mathbf{J}\cdot\mathbf{n}' > 0$ can be true, which has no physical sense. We assume that the flow density vector $\mathbf{J} = (0, 0, -\Phi)$ is parallel to the z axis. Having substituted it into integral (2), we obtain expression (4).

Parameters Λ, a, σ, μ and D are constant; i.e., they are independent of variables x, y, and t.

The anisotropic coefficients of the 4th derivatives in Eq. (3) are chosen so that the diffusion is isotropic within the target plane instead of the xy plane.

The problem formulation involves Eq. (3) that is solved in the rectangle $0 < x < H_x$, $0 < y < H_y$ for $t > 0$; the initial conditions are

$$h(x, y, 0) = -y \tan\theta + \eta(x, y), \tag{5}$$

where $\eta(x, y)$ is the given disturbance of the target plane surface; and the periodic boundary conditions are

$$h(x + H_x, y, t) = h(x, y, t), \quad h(x, y + H_y, t) = h(x, y, t) - H_y \tan\theta. \tag{6}$$

Note that here the ion flow density $\Phi(x, y, t)$ is a periodic function of variables x and y with periods H_x and H_y, respectively.

At $\Phi(x, y, t) = \Phi_0 = \text{const}$, $\eta(x, y) = 0$, the solution of problem (3)–(6) can be written in the following form:

$$h = -\frac{\Lambda\Phi_0}{\sqrt{2\pi(\sigma^2\cos^2\theta + \mu^2\sin^2\theta)}}\exp\left\{-\frac{a^2}{2(\sigma^2 + \mu^2\tan^2\theta)}\right\}t\eta(t) - y\tan\theta; \tag{7}$$

i.e., the surface remains plane at any instant. However, as shown in [2], this solution is unstable and prone to small disturbances of the surface morphology. Ripples with a specific wavelength are formed on the surface.

3. MODIFICATIONS OF THE MONTE CARLO METHOD

3.1. Method 1: Imitational Simulation

The ion flow density can be presented in the form of the sum of the densities of the flow of separate particles:

$$\Phi(x, y, t) = \sum_{k=1}^{N}\delta(x - x_k)\delta(y - y_k)\delta(t - t_k), \quad 0 < x < H_x, \quad 0 < y < H_y, \tag{8}$$

where $\delta(x)$ is the Dirac δ-function, x_k, y_k, and t_k is the sequence of random points uniformly distributed in the rectangular parallelepiped $0 < x < H_x$, $0 < y < H_y$, $0 < t < T$. Note that since $\Phi(x, y, t)$ is a periodic function of variables x and y with periods H_x and H_y, respectively, in each of the parallelepipeds

$$lH_x < x < (l + 1)H_x, \quad mH_y < y < (m + 1)H_y, \quad 0 < t < T, \tag{9}$$

where l and m are integers, the following set of N random points is selected: $x_k + lH_x$ and $y_k + mH_y$, t_k, and the ion flow density is

$$\Phi(x, y, t) = \sum_{k=1}^{N}\delta(x - x_k - lH_x)\delta(y - y_k - mH_y)\delta(t - t_k).$$

We can limit ourselves to integers $l = 0, \pm1$ and $m = 0, \pm1$ in the calculations since the integrand E in Eq. (4) rapidly vanishes with the increase in the distance between points (x, y) and (x', y').

We designate $x_{l,k} = x_k + lH_x$ and $y_{m,k} = y_k + mH_y$ and assume

$$\eta(x, y) \equiv 0. \tag{10}$$

in the initial condition (5).

Substitution of function (8) into integral (4) produces the following expression for the erosion velocity:

$$V_0(x, y, t) = \Lambda\sum_{k,l,m}E(x - x_{l,k}, y - y_{m,k}, \quad h(x, y, t) - h(x_{l,k}, y_{m,k}, t) + a)\delta(t - t_k). \tag{11}$$

To solve problem (3), (5), (6), (10), and (11), we apply the following numerical algorithm.

We set the uniform rectangular grid

$$\Pi = \{i\Delta x, j\Delta y\}, \quad i = 0\ldots N_x, \quad j = 0\ldots N_y, \quad \Delta x = H_x/N_x, \quad \Delta y = H_y/N_y \tag{12}$$

and approximate differential Eq. (3) with the following difference equation

$$\frac{h_{i,j}^{n+1} - h_{i,j}^{n}}{\tau} = -\tilde{V}_0\sqrt{\tilde{g}} - D(\Lambda_x[h_{i,j}^{n}] + \Lambda_y[h_{i,j}^{n}] + 2\Lambda_{x,y}[h_{i,j}^{n}]), \tag{13}$$

where τ is the time step,

$$\Lambda_x[h_{i,j}^{n}] = \frac{h_{i+2,j}^{n} - 4h_{i+1,j}^{n} + 6h_{i,j}^{n} - 4h_{i-1,j}^{n} + h_{i-2,j}^{n}}{(\Delta x)^4},$$

$$\Lambda_y[h_{i,j}^{n}] = \frac{h_{i,j+2}^{n} - 4h_{i,j+1}^{n} + 6h_{i,j}^{n} - 4h_{i,j-1}^{n} + h_{i,j-2}^{n}}{(\Delta y)^4}\cos^4\theta,$$

$$\Lambda_{xy}[h_{i,j}^{n}] = \frac{h_{i+1,j+1}^{n} + h_{i-1,j-1}^{n} + h_{i+1,j-1}^{n} + h_{i-1,j+1}^{n} - 2(h_{i+1,j}^{n} + h_{i,j+1}^{n} + h_{i-1,j}^{n} + h_{i,j-1}^{n}) + 4h_{i,j}^{n}}{(\Delta x\Delta y)^2}\cos^2\theta,$$

$$\tilde{g} = 1 + (\Delta_x h_{i,j}^{n}/\Delta x)^2 + (\Delta_y h_{i,j}^{n}/\Delta y)^2, \quad \Delta_x h_{i,j}^{n} = \min(0, h_{i,j}^{n} - h_{i-1,j}^{n}, h_{i,j}^{n} - h_{i+1,j}^{n})$$

$$\Delta_y h_{i,j}^{n} = \min(0, h_{i,j}^{n} - h_{i,j-1}^{n}, h_{i,j}^{n} - h_{i,j+1}^{n}),$$

$$\tilde{V}_0 = \Lambda\sum_{k,l,m} E(i\Delta x - x_{l,k}, j\Delta y - y_{m,k}, \overline{h}_{i,j}^{n} - h_{l,m,k} + a)(\eta((n+1)\tau - t_k) - \eta(n\tau - t_k))/\tau, \tag{14}$$

$\eta(t)$ is the Heaviside function,

$$\overline{h}_{i,j}^{n} = (h_{i,j}^{n} + h_{i+1,j}^{n} + h_{i-1,j}^{n} + h_{i,j+1}^{n} + h_{i,j-1}^{n})/5, \tag{15}$$

and h_{lmk} is the height of the target surface at the point (x_{lk}, y_{mk}), whose value is found by a bilinear interpolation of its values at the spatial grid points (12) on the temporal layer n with the application of the periodic boundary conditions (6). The summing up in the second member of formula (14) is actually made over all the ions incident onto the target between the temporal layers n and $(n + 1)$.

The difference equation (13) supplemented with the initial and boundary conditions (5)–(6) is a conditionally stable difference scheme. The following conditions are required for its stability:

$$D\tau\left[\frac{1}{(\Delta x)^2} + \frac{\cos^2\theta}{(\Delta y)^2}\right]^2 < \frac{1}{8}, \tag{16}$$

$$\frac{\Lambda}{(2\pi)^{3/2}\mu^2\sigma} < \Delta x/2, \quad \frac{\Lambda}{(2\pi)^{3/2}\mu^2\sigma} < \Delta y/2, \quad 2\pi\mu^2\Phi_0\tau < 1. \tag{17}$$

Inequality (16) formulates the difference scheme's stability condition without the nonlinear term $\tilde{V}_0\sqrt{\tilde{g}}$. Inequality (17) ensures the fulfillment of the estimation

$$\tilde{V}_0\sqrt{\tilde{g}}\,\tau \le \tilde{V}_0\tau + \frac{1}{2}\left|\Delta_x h_{i,j}^{n}\right| + \frac{1}{2}\left|\Delta_y h_{i,j}^{n}\right|.$$

3.2. Method 2: Quasi Monte Carlo

This method implements the same calculation scheme (13)–(15) as the first method with one exception. The sequence of random points (x_k, y_k) uniformly distributed in the rectangle $0 < x < H_x$, $0 < y < H_y$ is replaced by its determined analog—the Holton sequence [15]. In the two-dimensional case, the coordinates of points (p_k, q_k) of the Holton sequence uniformly distributed in a square are calculated by the following formulas:

$$p_k = \sum_{i=1}^{m} a_i \times 2^{-i}, \quad q_k = \sum_{i=1}^{n} b_i \times 3^{-i},$$

where $k = a_m a_{m-1},\ldots,a_1$ is the index written in the binary notation and $k = b_n b_{n-1},\ldots,b_1$ is the index written in the ternary notation.

For any natural numbers K, s, and l, exactly $[K/(N_xN_y)]$ or $[K/(N_xN_y)]+1$ points from the first K points of sequence (H_xp_k, H_yq_k) enter each cell $[i\Delta x,(i+1)\Delta x) \times [j\Delta y,(j+1)\Delta y)$ of the uniform rectangular grid (12) with parameters $N_x = 2^s$, $N_y = 3^l$. This specific feature ensures the best uniformity of the distribution of the Holton sequence of points in comparison with an independent random point sequence. Using the Holton sequence for the simulation of ion coordinates in the flow considerably reduces the fluctuations of the depth of the target sputtering but can cause the formation of additional ordered structures on the target surface.

Note. The Holton sequence is actually a sequence of multidimensional cubic points. These points can be effectively used for the estimation of multidimensional integrals of approximately regular functions over domains whose boundaries are composed of hyperplanes parallel to the coordinate planes; however, they are not suitable for studying stochastic systems. However, the boundary problem (3)–(6) and (10) can be considered in the form of a deterministic model. In this case, the use of cubic points to estimate integral (4) can be useful for the numerical solution of this problem.

3.3. Method 3: Rejection of the True Ion Trajectories

Integral (4) is presented in the following form:

$$V_0(x,y,t) = \frac{\Lambda\Phi_0}{\sqrt{2\pi}\sigma}\iint dx'dy' \exp\left\{-\frac{(h(x,y,t)-h(x',y',t)+a)^2}{2\sigma^2}\right\}\rho(x-x',y-y'), \tag{18}$$

where $\rho(x,y) = \dfrac{1}{2\pi\mu^2}\exp\left\{-\dfrac{x^2+y^2}{2\mu^2}\right\}$ and is considered as the mathematical expectation of the random quantity

$$\xi(h(x,y,t),h(x',y',t)) = \frac{\Lambda\Phi_0}{\sqrt{2\pi}\sigma}\exp\left\{-\frac{(h(x,y,t)-h(x',y',t)+a)^2}{2\sigma^2}\right\}, \tag{19}$$

distributed with density $\rho(x-x',y-y')$ near point (x,y).

In the numerical scheme (13), we draw the erosion velocity $\tilde{V}_0$ at each time step by the following formulas:

$$\tilde{V}_0 = \xi(\bar{h}_{ij}^n, h(x',y',n\tau)), \quad x' = i\Delta x + r\cos\varphi, \quad y' = j\Delta y + r\sin\varphi, \quad r = \mu\sqrt{-2\ln\gamma_1}, \quad \varphi = 2\pi\gamma_2, \tag{20}$$

where $\gamma_{1,2}$ are independent random numbers uniformly distributed over segment [0, 1] and are the same for all points (i,j) of the spatial grid. The target height is found at point (x',y') using the bilinear interpolation of its values at the spatial grid points (12) on temporal layer n.

Note that when the condition

$$\left|h(x,y,t)-h(x',y',t)+(y-y')\tan\theta\right| \ll a$$

is met, random quantity (19) weakly depends on coordinates x and y, so that the implementation of the calculation scheme (13) and (20) induces fluctuations in the depth of the target sputtering, which are smaller by several factors than the ones observed with the implementation of the numerical scheme (13) and (14). In addition, the initial condition (5) requires setting the initial disturbance of the target surface as $\eta(x,y) \neq \text{const}$. Otherwise, we obtain solution (7) and the surface remains plane at any instant.

Note. Methods 1 and 3 are fundamentally different formulations of the problem or different discrete analogs of the continuous model (3)–(6). They differ in the approaches to the discrete approximation of the nonlinear integral operator (4). The first method stipulates transition from integration to summation (11) for all particles (ions) incident onto the target. In the numerical calculations, the contribution of each ion to the proximal points of the grid is actually counted. This contribution tends to zero under the Gaussian law as the distance from the point of ion interaction with the surface of the target grows. The third method implies that for every point of the computational grid, there is a set of ions whose coordinates are drawn according to the same Gaussian law and smoothly vary with the transit to the next points of the grid. We still need to study carefully, which of the specified approaches to discretize the integral operator is the most successful. These studies can be performed by the calculation experiments. In any case, the expediency of using the Monte Carlo method is dictated by the dimension of the problem, which consid-

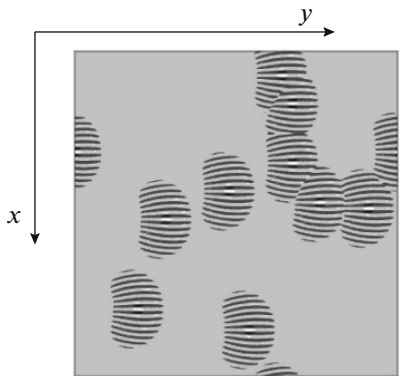

Fig. 1. Oblique incidence (22). Third Monte Carlo method. Temporal layer $n = 50000$. $M = 10$. Surface width $W = 4.15 \times 10^{-4}$.

ers the discretization over five variables x, y, x', y' and t. Fine grids are required for variables x and y, and the number of temporal layers can reach 6–7 orders.

4. DESCRIPTION OF THE CALCULATION EXPERIMENT

The developed computing circuits are implemented on the computing resources of the Interdepartmental Supercomputer Center of the Russian Academy of Sciences. The corresponding program codes were run at the MSC-100k multiprocessing computing system using MPI functions. The geometrical method of parallelizing was applied. The calculated space was divided into pairwise intersecting bands parallel to the y axis. The minimum bandwidth was bounded below to a value equal to the maximum distance between a point of the space grid and a point of the ion interaction with the surface.

The following parameters were used in the calculations:

$$a = 1/6, \quad \sigma = \mu = 1/3, \quad \frac{\Lambda\Phi_0\tau}{\sqrt{2\pi\sigma}} = 0.002, \quad D\tau = 2\times10^{-5}, \quad N_x \times N_y = 1250\times1250. \tag{21}$$

Two modes of the ionic irradiation of the surface were considered:

(1) Oblique incidence

$$\tan\theta = 1/2, \quad H_x = 200, \quad H_y = 175; \tag{22}$$

(2) Normal incidence

$$\tan\theta = 0, \quad H_x = 200, \quad H_y = 200. \tag{23}$$

In the implementation of the Monte Carlo method's third modification (13) and (20), the initial disturbance of the target surface was set in the following form:

$$\eta(x,y) = 0.01\sum_{s=1}^{M}\delta_{i_s,j_s}, \quad \delta_{ij} = \begin{cases}1, & i = j,\\ 0, & i \neq j,\end{cases} \tag{24}$$

where (i_s, j_s) are the disturbed points of the spatial grid selected randomly.

The surface morphology of the target was presented by the following function:

$$u(x,y,t) = h(x,y,t) + y\tan\theta + h_0(t), \tag{25}$$

where $h_0(t) = -\dfrac{1}{H_xH_y}\displaystyle\int_0^{H_y}\int_0^{H_x}(h(x,y,t) + y\tan\theta)dxdy$ is the mean depth of the target sputtering.

5. RESULTS OF CALCULATIONS AND DISCUSSIONS

5.1. Oblique Incidence (22)

In Figs. 1 and 2, the results of the calculations of function (25) by the third Monte Carlo method (13) and (20) are presented at the time when the longitudinal ripples are generated on the surface of the target.

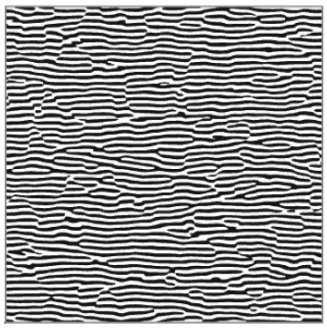

Fig. 2. Oblique incidence (22). Third Monte Carlo method. Temporal layer $n = 50000$. $M = 1000$. Surface width $W = 4.33 \times 10^{-3}$.

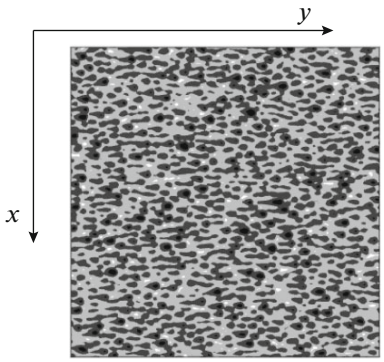

Fig. 3. Oblique incidence (22). First Monte Carlo method. Temporal layer $n = 50000$. $\Phi_0\tau = 0.1$. Surface width $W = 0.455$.

Here, Fig. 1 corresponds to the initial disturbance of $M = 10$ points of the space grid by formula (24) and Fig. 2 corresponds to the initial disturbance of $M = 1000$ grid points. The light background corresponds to positive values of function (25) and the dark background shows the negative values of this function. The degree of roughness of the target surface can be quantitatively described by the magnitude termed as the surface width calculated by formula [2]:

$$W(t) = \sqrt{\frac{1}{H_x H_y}\int_0^{H_y}\int_0^{H_x} u^2(x,y,t)dxdy}\cos\theta. \tag{26}$$

This magnitude is $W = 4.15 \times 10^{-4}$ and $W = 4.33 \times 10^{-3}$ for the results presented in Figs. 1 and 2, respectively.

In Figs. 3 and 4, the results of similar calculations by the first and the second Monte Carlo methods, respectively, are imaged. Note that the initial disturbance of the surface of the target in these cases is zero (see (10)). However, for the first and the second methods, in addition to parameters (21), we need to set the ion flow density $\Phi_0\tau$ per time step, since these methods presume the simulation of the actual paths of ions. For the results presented in Figs. 3 and 4, this parameter is $\Phi_0\tau = 0.1$. Such a choice of this parameter corresponds to the calculation time approximately equal to the time of similar calculations by the third method.

Comparing the results presented in Figs. 1–4 we see random fluctuations, which blur the wave structure (see Fig. 3), developing on the surface of the target when using imitational simulation (method 1). The use of the quasi-Monte Carlo method (method 2) considerably reduces fluctuations of the depth of the target sputtering but causes a resonance effect of the interaction between the wave structure on the surface of the target and the structure of the Holton sequence used to simulate ion paths (see Fig. 4). The refusal to simulate the actual ion paths (method 3) allows eliminating the disadvantages of the first and the second methods and to obtain the limiting pattern best corresponding to the continuous model (3)–(6) (see Figs. 1, 2).

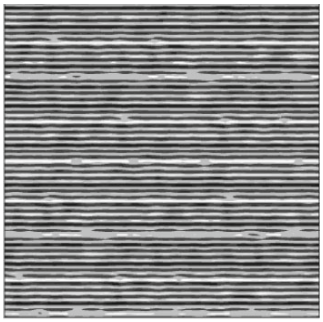

Fig. 4. Oblique incidence (22). Second Monte Carlo method. Temporal layer $n = 50000$. $\Phi_0\tau = 0.1$. Surface width $W = 0.205$.

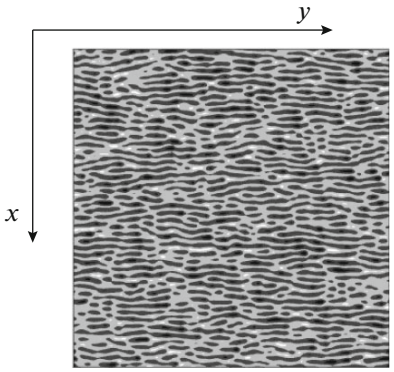

Fig. 5. Oblique incidence (22). First Monte Carlo method. Temporal layer $n = 50\,000$. $\Phi_0\tau = 10$. Surface width $W = 0.255$.

Note, however, that the imitating simulation (method 1) shows better agreement with the considered physical process. We need to set the Λ and Φ_0 parameters accurately to obtain its adequate description. The continuous model is the limiting case with $\Phi_0 \to \infty$, $\Lambda\Phi_0 = \text{const}$.

In Fig. 5, the results of the calculations of function (25) by method 1 are presented at a different ion flow density $\Phi_0\tau = 10$ but the same parameters (21) of the erosion and diffusion velocities. These results show the longitudinal ripples on the surface of the target. However, note that a hundred-fold increase of the ion flow density under the condition of $\Lambda\Phi_0 = \text{const}$ demands a hundred-fold increase of the calculation time by the first Monte Carlo method.

The wavelength of the ripples and their orientation on the surface of the target can be determined by the structural factor. The structural factor $S(\mathbf{q}, t)$ is calculated by applying the Fourier transformation of the function $u(x, y, t)$ under the following formulas [2]:

$$S(\mathbf{q},t) = \left|h(\mathbf{q},t)\right|^2,$$

where $h(q,t) = \iint \frac{dxdy}{(2\pi)^2} u(x,y,t)\exp(iq_x x + iq_y y)$.

The ripple wavelength corresponds to the maximum value of the structural factor.

In Figs. 6–8, the structural factor is shown as a function of coordinates q_x and q_y of the wave vector on the temporal layer $n = 50\,000$ for the results presented in Figs. 2, 4, and 5. In these figures, two peaks are observed at the wave vector coordinates corresponding to its orientation parallel to the x axis, i.e., corresponding to the formation of the longitudinal ripples. The narrow peaks in Fig. 7 indicate the longitudinal ripples' wavelength resonance on the target surface with the corresponding wavelength of the flow density of the ions whose paths are simulated by the Holton sequence in the Monte Carlo method's second modification. This circumstance, on the one hand, shows that application of the Holton sequence can produce distorted results, an on the other hand, it shows that the observed resonance allows us to calculate precisely the wavelength of the longitudinal ripples on the target surface: $\lambda = 2\pi/q_x \approx 4.17$.

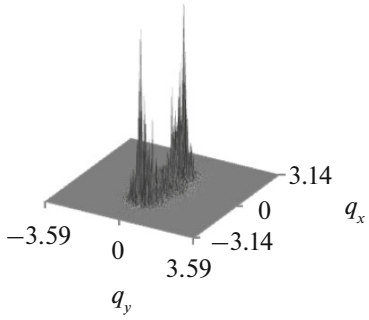

Fig. 6. Oblique incidence (22). Structural factor as function of wave vector on q_x and q_y coordinates on temporal layer $n = 50000$ for results shown in Fig. 5.

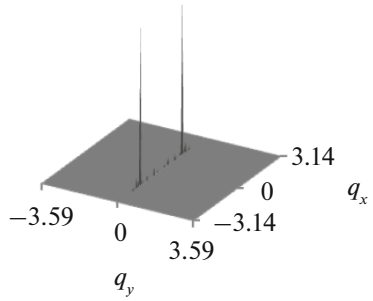

Fig. 7. Oblique incidence (22). Structural factor as function of wave vector on q_x and q_y coordinates on temporal layer $n = 50000$ for results shown in Fig. 4.

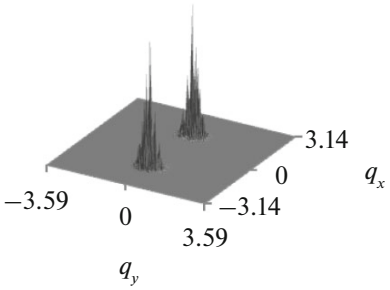

Fig. 8. Oblique incidence (22). Structural factor as function of wave vector on q_x and q_y coordinates on temporal layer $n = 50000$ for results shown in Fig. 2.

In [2], model (1) and (2) was analyzed in the linear approximation. In the symmetrical case of $\sigma = \mu$, when condition

$$D \gg D_0 = Fa\sigma^2/8$$

is met, where $F = \dfrac{\Lambda\Phi_0}{\sqrt{2\pi}\sigma}\exp\left\{-\dfrac{a^2\cos^2\theta}{2\sigma^2}\right\}$, the following relation is obtained

$$a/\sigma < \sqrt{2/\cos^2\theta}, \tag{27}$$

which induces longitudinal ripples with the wavelength

$$\lambda = 2\pi\sqrt{\frac{2D}{|v_x|}}, \quad v_x = -\frac{Fa}{2}\cos^2\theta. \tag{28}$$

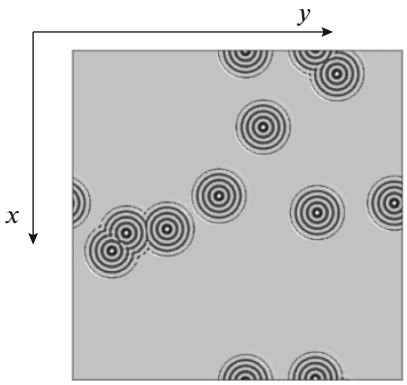

Fig. 9. Normal incidence (23). Third Monte Carlo method. Temporal layer $n = 50000$. $M = 10$. Surface width $W = 1.87 \times 10^{-2}$.

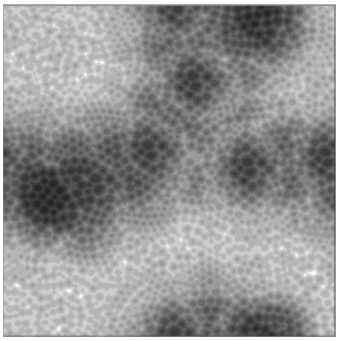

Fig. 10. Normal incidence (23). Third Monte Carlo method. Temporal layer $n = 200000$. $M = 10$. Surface width $W = 1.73$.

Relation (28) can be used to estimate the wavelength in our case. For the chosen values of parameters (21), inequality $D/D_0 = 4.77 > 1$ is true, relation (27) is valid for any angles θ, and the wavelength of the longitudinal ripples is $\lambda = 3.62 \sim 4$.

We have performed numerical calculations using the third method for smaller values of the angle of incidence of the ion beam, and estimated the calculation error by comparing our results with the results obtained for different steps of the computation grid. At all angles θ, the longitudinal ripples corresponding to the wave's vector orientation parallel to the x axis were formed on the target surface. The error of the results presented in Figs. 1 and 2 is about 1% of the maximum absolute value of function (25). On violation of conditions (16) and (17) and on the rejection of averaging (15), the difference scheme lost its stability.

5.2. Normal Incidence (23)

In Fig. 9–11, the target surface morphology obtained by the third Monte Carlo method (13) and (20) is shown at the normal incidence of the ion beam. The images in Figs. 9 and 10, correspond to $M = 10$ (ten point disturbances in the starting condition (24)). These figures show the initial stage of shaping the target surface morphology. In Fig. 11, the morphology of the target surface after a lengthy exposure to the normal ion beam is displayed; here, the number of point disturbances is assumed to be $M = 1000$ in the formula of the initial condition (24). This figure shows the sections of the surface with a self-organized ordered structure from the hollows (black points) with hexagonal symmetry. The autocorrelation function for one such section is presented in Fig. 12.

The results of similar calculations obtained by the first and the second Monte Carlo methods for the ion beam density $\Phi_0\tau = 0.1$ are presented in Figs. 13–16.

Figures 13 and 14 refer to the same time as the results presented in Figs. 1–5 for the ion beam's oblique incidence; and Fig. 9, for the normal incidence of ions. Having analyzed the results, we can conclude that at the normal incidence of the ions, no wave structure is formed on the target surface at the specified

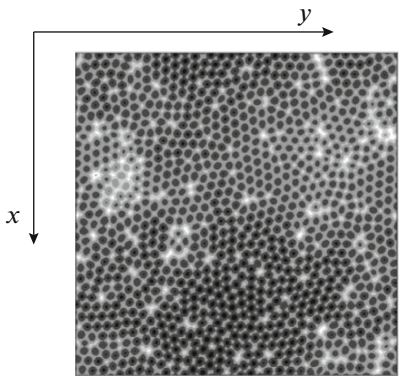

Fig. 11. Normal incidence (23). Third Monte Carlo method. Temporal layer $n = 5000000$. $M = 1000$. Surface width $W = 0.676$.

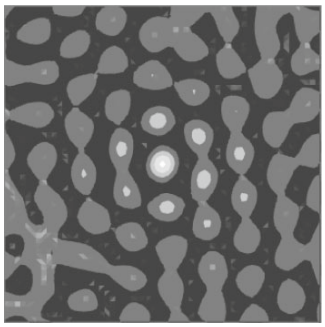

Fig. 12. Normal incidence (23). Autocorrelation function for results shown in Fig. 11.

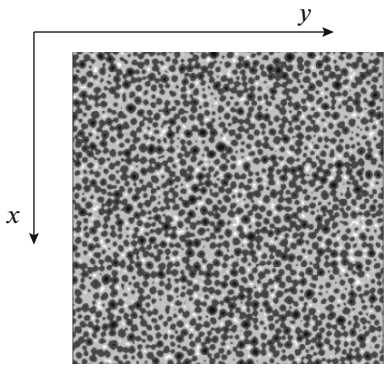

Fig. 13. Normal incidence (23). First Monte Carlo method. Temporal layer $n = 50000$. $\Phi_0\tau = 0.1$. Surface width $W = 0.54$.

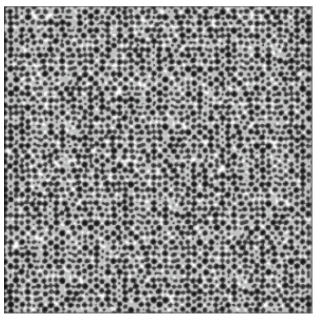

Fig. 14. Normal incidence (23). Second Monte Carlo method. Temporal layer $n = 50000$. $\Phi_0\tau$=0.1. Surface width $W = 0.343$.

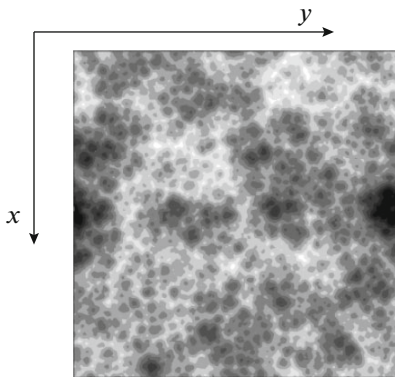

Fig. 15. Normal incidence (23). First Monte Carlo method. Temporal layer $n = 5000000$. $\Phi_0\tau = 0.1$. Surface width $W = 2.05$.

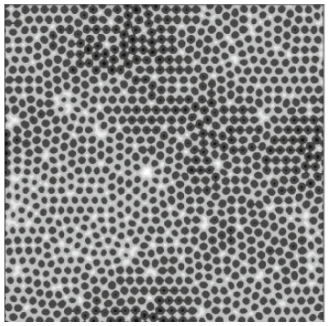

Fig. 16. Normal incidence (23). Second Monte Carlo method. Temporal layer $n = 5000000$. $\Phi_0\tau = 0.1$. Surface width $W = 0.565$.

instant. Some orderliness of the points is observed in the results obtained by the second method using the Holton sequence due to the periodic properties of this sequence.

In Figs. 15 and 16, the morphology of the target surface is shown obtained upon a lengthy exposure to irradiation according to the first and the second Monte Carlo methods. The surface morphology illustrated in Fig. 16 and obtained by the second method (the quasi-Monte Carlo) is similar to the surface morphology displayed in Fig. 11 and shows the formation of an ordered structure from hollows with hexagonal symmetry. In Fig. 15, the random fluctuations of the depth of the target surface sputtering, which are characteristic of the imitating simulation (method 1) cause the roughening of this surface with width $W = 2.05$, which several times exceeds the corresponding results presented in Figs. 11 and 16.

In order to reduce the random fluctuations by two orders of magnitude, we need to increase the density of the ion beam flow and the corresponding volume of the calculations by 3–4 orders of magnitude. With our limited computing resources, such calculations are a challenge, since obtaining the results for the long exposure to irradiation is a rather demanding procedure. Hence, for the numerical studies of a continuous model (3)–(6), it is more expedient to use the second (quasi-Monte Carlo) and the third (rejection of the actual paths) modifications of the Monte Carlo method. The third modification of the Monte Carlo method is preferable, since using the Holton sequence to model the ion coordinates in the second method induces the formation of additional ordered structures on the target surface.

6. CONCLUSIONS

The numerical study of the continuous model (3)–(6) of ionic sputtering of amorphous surfaces carried out in this paper by the Monte Carlo methods allows the following conclusions to be drawn.

Direct (imitational) statistical simulation of the ionic bombardment of the target surface, fit closest to the considered physical process and are widely used in other papers, has a significant disadvantage in that the ordered structures on the target surface are observed in the limiting case $\Phi_0 \to \infty$, $\Lambda\Phi_0 = \text{const}$, which requires huge computing resources. The random fluctuations of the depth of the sputtering of the target

surface, which are characteristic of the imitational simulation, cause the surface to roughen to such an extent that it prevents us from observing the modes resulting from the continuous model (1)–(2). This is particularly true for the modes set after a lengthy exposure of the target surface to the ionic irradiation when the strong nonlinearity significantly influences the morphology of the irradiated surface. These solutions are difficult for the theoretical analysis.

However, the solutions of the continuous model (3)–(6) can be examined numerically by other Monte Carlo method modifications with decreased dispersion. Two modifications are developed in this paper. With their help, the ordered structure is formed from hexagonally symmetrical hollows after the exposure of the target surface to irradiation by a normal ion beam under certain conditions for a long time.

ACKNOWLEDGMENTS

The study was supported by the Russian Science Foundation, project no. 14-11-00258 to support studies accomplished by individual research groups.

REFERENCES

1. N. N. Gerasimenko and Yu. N. Parkhomenko, *Silicon is the Material of Nanotechnologies* (Tekhnosfera, Moscow, 2007) [in Russian].
2. M. A. Makeev, R. Cuerno, and A.-L. Barabasi, "Morphology of ion sputtered surfaces," Nucl. Instrum. Methods Phys. Res. B **197**, 185–227 (2002).
3. S. Park, B. Kahng, H. Jeong, and A.-L. Barabasi, "Dynamics of ripple formation in sputter erosion: nonlinear phenomena," Phys. Rev. Lett. **83**, 3486 (1999).
4. B. Kahng, H. Jeong, and A.-L. Barabasi, "Quantum dot and hole formation in sputter erosion," Appl. Phys. Lett. **78**, 805–807 (2001).
5. M. Feix, A. K. Hartmann, R. Kree, J. Munoz-Garcia, and R. Cuerno, "Influence of collision cascade statistics on pattern formation of ion-sputtered surfaces," Phys. Rev. B **71**, 125407 (2005).
6. N. A. Kudryashov, P. N. Ryabov, T. E. Fedyanin, and A. A. Kutukov, "Evolution of pattern formation under ion bombardment of substrate," Phys. Lett. A **377**, 753–759 (2013).
7. N. A. Kudryashov and P. N. Ryabov, "Exact solutions of one pattern formation model," Appl. Math. Comput. **232**, 1090–1093 (2014).
8. P. Sigmund, "Sputtering by particle bombardment," Top. Appl. Phys. **47**, 9–71 (1981).
9. G. A. Mikhailov and A. V. Voitishek, *Numerical Statistical Modelling. Monte-Carlo Methods* (Akademiya, Moscow, 2006) [in Russian].
10. S. M. Ermakov, *Monte-Carlo Method in Computational Mathematics, Introductory Course* (St. Petersburg, 2009) [in Russian].
11. I. M. Sobol, *Numerical Monte-Carlo Methods* (Nauka, Moscow, 1973) [in Russian].
12. E. O. Yewande, A. K. Hartmann, and R. Kree, "Propagation of ripples in Monte Carlo models of sputter-induced surface morphology," Phys. Rev. B **71**, 195405 (2005).
13. A. K. Hartmann, R. Kree, and T. Yasseri, "Simulating discrete models of pattern formation by ion beam sputtering," J. Phys.: Condens. Matter **21**, 224015 (2009).
14. N. A. Kudryashov and M. V. Skachkov, "Statistical simulation of pattern formation by ionbeam sputtering," Multidiscip. Model. Mater. Struct. **11**, 527–543 (2015).
15. H. Niederreiter, *Random Number Generation and Quasi-Monte Carlo Methods* (SIAM, Philadelphia, PA, 1992).

Translated by N. Semenova